



# Catalytic activity of dendrimer encapsulated Pt nanoparticles anchored onto carbon towards oxygen reduction reaction in polymer electrolyte fuel cells

Tintula Kottakkat, Akhila K. Sahu\*, Santoshkumar D. Bhat, Pitchumani Sethuraman, Sridhar Parthasarathi

CSIR-Central Electrochemical Research Institute – Madras Unit, CSIR Madras Complex, Taramani, Chennai, 600 113, India

## ARTICLE INFO

### Article history:

Received 13 June 2011

Received in revised form 30 August 2011

Accepted 31 August 2011

Available online 7 September 2011

### Keywords:

PAMAM dendrimers

Pt nano-catalyst

Oxygen reduction reaction

PEFCs

## ABSTRACT

Pt nanoparticles are encapsulated in the fourth-generation hydroxyl-terminated poly (amidoamine) (PAMAM) dendrimer (G4-OH) and anchored onto carbon to realize a novel cathode catalyst for polymer electrolyte fuel cells (PEFCs). Extensive physical and electrochemical characterizations confirm that Pt/G4-OH-C catalyst exhibits significant enhancement of catalytic activity towards oxygen reduction reaction (ORR). The mass activities ( $A \text{ mg}_{\text{Pt}}^{-1}$ ) at 0.9 V vs. RHE for Pt/G4-OH-CI and Pt/G4-OH-CII, both prepared by different routes, are enhanced by 3.6 and 2.6 times, respectively, in relation to Pt/C catalyst. Dendrimer template studied here provides size-controlled preparation of Pt-based catalyst and facilitates uniform dispersion and loading of the catalyst onto carbon support. It is noteworthy that a PEFC comprising Pt/G4-OH-C catalyst with a Pt loading of  $\sim 0.1 \text{ mg cm}^{-2}$  delivers a power density of  $712 \text{ mW cm}^{-2}$  at 0.6 V with  $\text{H}_2$  and  $\text{O}_2$  feeds. By contrast, the PEFC using Pt/C with a Pt loading of  $\sim 0.2 \text{ mg cm}^{-2}$  delivers a power density of only  $370 \text{ mW cm}^{-2}$  while operating under similar conditions.

© 2011 Elsevier B.V. All rights reserved.

## 1. Introduction

Nanomaterials are being projected for integration with advanced energy-storage and conversion devices, namely batteries, supercapacitors and fuel cells [1]. Platinum is used as the catalyst material in most of the low-temperature fuel cells. But since the global supplies of platinum are limited, there is a definite need to reduce its loadings to make the catalyst cost-effective. An effective way of reducing the platinum loadings without sacrificing the performance is to adapt nano-platinum particulates as catalyst in fuel cells. But while doing so, the effects of miniaturization, quantum size-effects, and the physical properties of small atoms vis-à-vis bulk metals, need to be tackled [2,3]. Extreme miniaturization of Pt particles to nanometers scale may drastically change the characteristics of the particles favourably or unfavourably. Although a definitive answer to this problem is still lacking, several reports predict a particle-size limit of about 3 nm [4–6]. Accordingly, strategies for the production of discrete metal clusters with precise size control are being directed on the manipulation of metallic components at the atomic levels. A method for preparation is therefore required where the metal particle-size is controlled along with uniform distribution in a discrete manner. Polymers with highly branched monodispersed macromolecules, such as

dendrimers, have drawn considerable interest in medicine, nanotechnology and catalysis due to their unique structure, surface reactivity and desirable physico-chemical properties of the encapsulated nanoparticles [7–9]. The ability to control interior/exterior functionalities of dendrimers and the macromolecular architecture with open spaces within the interior creates an ideal environment for trapping guest species [10–12]. Specifically, Poly (amidoamine) (PAMAM) dendrimers can bind a defined number of transition-metal cations and thus template and stabilize metal oxide or metal nanoparticles [13,14]. An attractive approach by Crooks and co-workers which uses PAMAM dendrimers is recognized for the size-controlled synthesis of nanoparticles on a single nanometre scale and can be extended to Pt [15–18]. The conventional catalyst layers in PEFCs generally have high platinum loadings of up to about  $0.5 \text{ mg cm}^{-2}$  to surmount the kinetic limitation at the cathode which makes it cost intensive [19,20]. In order to surmount these problems, it is necessary to maximize the activity of a Pt-based catalyst by tailoring its morphology and/or composition to acquire an electrocatalyst with adequate surface area and activity [21,22].

Attempts have been made to reduce the Pt content in fuel cells: (a) by fabricating smaller particles to increase the Pt utilization and (b) by preventing the aggregation of Pt nanoparticles. However, the particle size remains limited in the catalysts prepared by the conventional preparative methods and functionalities of the supporting materials. To obviate the aforesaid issues, stabilizers such as surfactants, polymers and dendrimers are utilized to suppress aggregation and to control particle size [23–29]. Dendrimers

\* Corresponding author. Tel.: +91 44 22542068, fax: +91 44 22542456.

E-mail address: [akhilakumar2008@gmail.com](mailto:akhilakumar2008@gmail.com) (A.K. Sahu).

have an intrinsically well-defined globular structure and highly modifiable surface groups. Dendrimers are monodispersed building blocks, ideal guest-molecule carriers, promising bio-compatible materials and excellent templates for generating metal nanoparticles within their spacious interior [11,12,15,30–32]. Dendrimer templates have fairly uniform composition and structure, and therefore yield well-defined nanoparticle replicas. The nanoparticles are stabilized by encapsulation within the dendrimers and hence do not agglomerate. The encapsulated nanoparticles are confined primarily by steric effects and hence a substantial fraction of their surface is unpassivated and is available to participate in catalytic reactions [15,33–35]. Ye and Crooks [18] have demonstrated the electrocatalytic activity of Pt–Pd bi-metallic nanoparticle encapsulated with sixth-generation hydroxyl-terminated-PAMAM dendrimers (G6-OH) towards oxygen reduction reaction (ORR) with a mass activity of  $9.6 \text{ mA } \mu\text{g}_{\text{Pt}}^{-1}$  at 0.7 V vs. RHE. Pt–Ru deposited on G4-NH<sub>2</sub> PAMAM dendrimer functionalized carbon nano-fibre and is found to exhibit improved performance towards methanol oxidation as compared to commercial 20 wt% Pt–Ru on carbon [36]. This process may lead to dispersion of Pt on dendrimer surface and interior as well as on the carbon support. Impregnating metal particles first to the dendrimer and subsequently on carbon is seminal in providing better control on metal particle-size in the catalyst.

This study provides a facile method for encapsulating Pt nanoparticles in fourth-generation hydroxyl-terminated PAMAM dendrimers (G4-OH) and forming a composite with carbon nano-materials as a catalyst support. Better dispersion and utilization of Pt nanoparticles is achieved by hydroxyl-terminated PAMAM dendrimers, which acts both as a template and a stabilizer to synthesize Pt nanoparticles. The catalyst prepared in this study exhibits a significant enhancement in electrocatalytic activity towards ORR and fosters a better understanding on the catalyst utilization.

## 2. Experimental

### 2.1. Materials

Generation 4 PAMAM-OH dendrimer (G4-OH, 10 wt% solution in MeOH) was obtained from Sigma–Aldrich. The compounds K<sub>2</sub>PtCl<sub>4</sub>, Ethyl-(N, N-dimethylamino) propylcarbodiimide hydrochloride (EDC) and 4-(N, N-dimethylamino) pyridine (DMAP) were purchased from Acros Organics. The cellulose dialysis sacks (molecular weight cut off of 12,000) were purchased from Thermo-Fischer. Vulcan XC-72 carbon was obtained from Cabot Corporation. Milli-Q water (18 MΩ cm) was used to prepare aqueous samples.

### 2.2. Synthesis of dendrimer-encapsulated Pt nanoparticles on carbon

G4-OH dendrimers were used as templates to synthesize dendrimer-encapsulated Pt nanoparticles similar to the process described elsewhere [37]. Typically, about 10 mL of 0.5 mM G4-OH aqueous solution and 66.6 mL of 3 mM K<sub>2</sub>PtCl<sub>4</sub> aqueous solution were mixed together and stirred for 72 h in an inert atmosphere to ensure complete complexation of Pt<sup>2+</sup> with the interior tertiary amines (G4-OH-Pt<sup>2+</sup>) of the dendrimer. About 0.138 g of acid functionalized carbon (Vulcan XC-72) was dispersed in water and then mixed with G4-OH-Pt<sup>2+</sup> complex in the presence of defined quantity of EDC and DMAP as coupling reagents in a pH range of 4–6. The admixture was stirred for 10 h for forming G4-OH-Pt<sup>2+</sup>-C composite. The resultant G4-OH-Pt<sup>2+</sup>-C nano-composite was copiously washed with water and centrifuged for several times to remove excess G4-OH-Pt<sup>2+</sup> and uncomplexed Pt salt. The composite was

then dispersed in water and purged with nitrogen to remove the dissolved oxygen. Finally, 10 molar excess of freshly prepared aqueous NaBH<sub>4</sub> solution was added and stirred vigorously for 1 h. The resultant composite was washed with water and centrifuged for several times to remove the excess NaBH<sub>4</sub> and dried under vacuum at 60 °C. The catalyst synthesized by this route is hereafter represented as Pt/G4-OH-Cl. An alternative synthetic procedure was also adopted to ensure the Pt encapsulation inside the dendrimer cavity as follows. From the G4-OH-Pt<sup>2+</sup> complex, Pt<sup>2+</sup> was first reduced to its metallic state by NaBH<sub>4</sub> solution to obtain Pt/G4-OH. The excess salt was removed and then the Pt/G4-OH was supported onto carbon followed by washing with water and centrifuging several times till it reached neutral pH. The catalyst synthesized by this route is hereafter represented as Pt/G4-OH-CII. The schematic representation of the two synthesis route is shown in Fig. 1.

### 2.3. Physico-chemical characterizations

Complexation process for the samples was monitored at room temperature (25 °C) using UV–visible spectrophotometer (Shimadzu Corporation, Japan) with quartz cuvettes of 1 cm path length. All spectra were background corrected using spectrum obtained from an identical cell filled with de-ionized water and/or aqueous G4-OH solution. The presence of dendrimers on the surface of carbon support was confirmed by Fourier transform infrared (FTIR) spectroscopy (Thermo Nicolet, model Nexus 670) using KBr pellet method. Pt loading in the catalysts was determined by gravimetric analysis for various samples, namely Pt/C, Pt/G4-OH-Cl and Pt/G4-OH-CII, as follows. Approximately 10 mg of samples were heat-treated in a tubular furnace in air with heating ramps of 10 °C min<sup>-1</sup> from 25 to 800 °C and then kept at 800 °C for 30 min. Samples were allowed to cool to 200 °C in nitrogen atmosphere and purged with hydrogen to reduce Pt to its metallic state. The Pt loading was estimated from the weight difference of the samples. The Pt loading in the catalysts were also confirmed by inductively coupled plasma-optical emission spectroscopy (ICP-OES) from Perkin–Elmer. Transmission electron microscope (TEM) images were obtained using a 200 kV Tecnai-20 G2 for analyzing the Pt particle size and dispersion in the supporting material. For these measurements, the samples were suspended in acetone with ultrasonic dispersion for 3 min. Subsequently, a drop of this suspension was deposited on a holey carbon grid and allowed for drying. Images were recorded with a Multiscan CCD camera (model 794, Gatan) using low-dose conditions.

### 2.4. Electrochemical characterization

Electrochemical properties of the catalysts were measured by cyclic voltammetric (CV) and rotating disk electrode (RDE) analysis using an Autolab PGSTAT 30 (Eco-Chemie) at room temperature (25 °C). Catalyst suspension was prepared by ultrasonically dispersing 17–30 mg catalyst in 10 mL of an aqueous solution with a 10 wt% Nafion solution (DuPont) for 30 min. 10 μL aliquot of the suspended ink was dispersed on to 1.5 mm carbon disk electrode and dried at room temperature to obtain a Pt loading of  $\sim 36 \mu\text{g cm}^{-2}$ . A Pt wire and a saturated calomel electrode (SCE) were used as counter and reference electrodes, respectively in a standard three-electrode electrochemical cell. All potentials are reported in terms of the reversible hydrogen electrode (RHE) scale for convenience. Linear sweep voltammetry (LSV) for ORR measurements was performed in aqueous 0.5 M HClO<sub>4</sub> saturated with O<sub>2</sub> at a scan rate of 2 mV s<sup>-1</sup> with a rotation speed of 1600 rpm. Hydrogen adsorption–desorption voltammograms were recorded in 0.5 M HClO<sub>4</sub> aqueous solution at a scan rate of 50 mV s<sup>-1</sup> purging

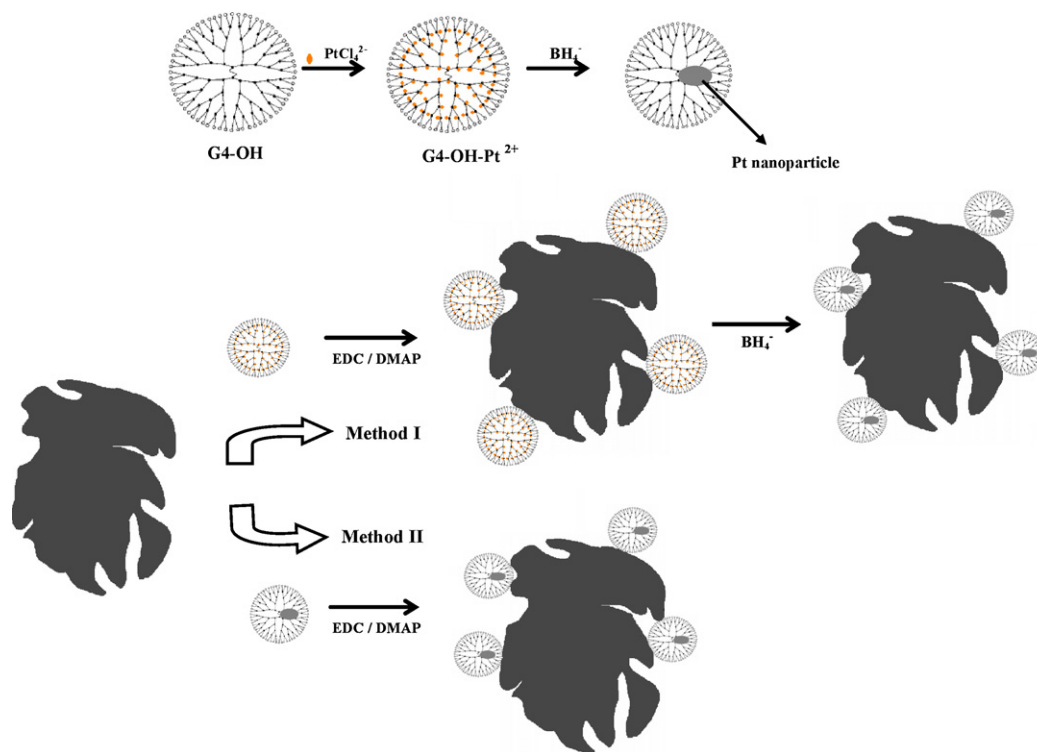


Fig. 1. Scheme representing the Pt nanoparticle encapsulation into G4-OH dendrimer and their subsequent incorporation onto carbon support.

with  $\text{N}_2$  gas to remove dissolved  $\text{O}_2$ . The region for hydrogen adsorption between 0.05 V and 0.4 V vs. RHE on the backward potential scan was used to estimate the electrochemical surface area (ESA).

### 2.5. Electrode fabrication and fuel cell performance evaluation

15 wt% teflonized Toray TGP-H-120 carbon papers of 0.37 mm thick were used as the backing layers. To prepare gas-diffusion layers (GDLs), Vulcan XC-72 carbon was suspended in cyclohexane and agitated in an ultrasonic water bath for 30 min. To this solution, 15 wt% PTFE (polytetrafluoroethylene) suspensions in 2 mL ammonia was added with continuous agitation to form a slurry to coat on the backing layer uniformly until the required loading of  $1.5 \text{ mg cm}^{-2}$  was attained. The GDL thus obtained was sintered in a furnace at  $350^\circ\text{C}$  for 30 min. For the reaction layer, prepared catalysts (Pt/G4-OH-CI and Pt/G4-OH-CII) were dispersed separately in isopropyl alcohol and ultra-sonicated for 30 min followed by the addition of 30 wt% of Nafion solution; the resultant slurries were ultra-sonicated for 1 h and coated onto the GDLs (represented as cathode) until a required Pt loading was achieved. For the anode, 20 wt% Pt/C (Johnson Matthey) was used with 7 wt% of Nafion loading. Membrane electrode assemblies (MEAs) were obtained by sandwiching the pre-treated Nafion-212 membranes between anodes and cathodes followed by hot compaction under a pressure of  $60 \text{ kg cm}^{-2}$  at  $130^\circ\text{C}$  for 3 min. MEAs were coupled with Teflon gas-sealing gaskets and placed in single-cell test fixtures with a parallel serpentine flow field machined on graphite plates. Gaseous  $\text{H}_2$  and gaseous  $\text{O}_2$  were fed to the anode and cathode of the PEFCs, respectively, through the bubble humidifiers kept at  $10^\circ\text{C}$  higher than the cell temperature. The flow rates of both the reactants were kept at  $100 \text{ mL min}^{-1}$ . After equilibration at a cell temperature of  $60^\circ\text{C}$ , galvanostatic polarization data were obtained using an LCN100-36 electronic load from Bitrode Corporation, US. All the MEAs were evaluated with an active area of  $4 \text{ cm}^2$  in PEFCs under atmospheric pressure.

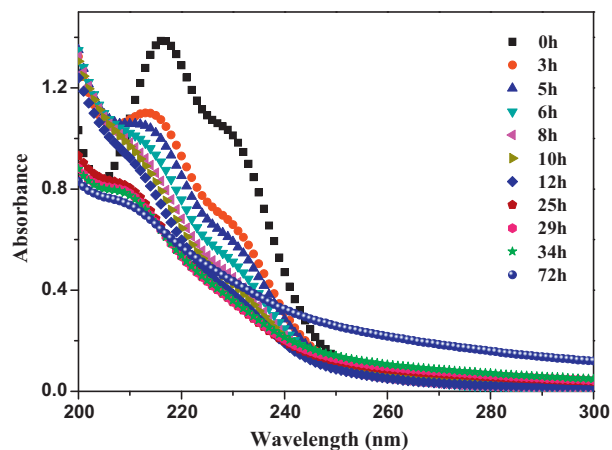
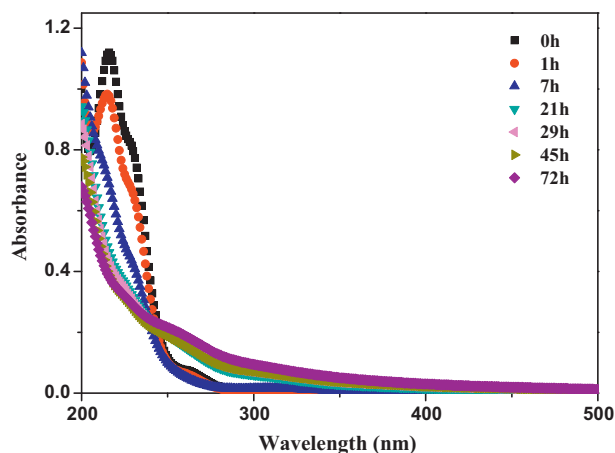


Fig. 2. Time-resolved UV-vis spectra showing the hydrolysis of  $120 \mu\text{M}$   $\text{K}_2\text{PtCl}_4$  solution.

### 3. Results and discussion

For co-ordination of  $\text{Pt}^{2+}$  to the interiors of G4-OH dendrimer,  $\text{K}_2\text{PtCl}_4$  is used as the  $\text{Pt}^{2+}$  precursor in the present study.  $\text{K}_2\text{PtCl}_4$  on hydrolyzing with water forms a complex with G4-OH [38,39]. Time-resolved UV-vis studies are carried out to confirm  $\text{PtCl}_4^{2-}$  hydrolysis and subsequent binding of the hydrolysed product to the tertiary amine groups of the G4-OH dendrimer. Fig. 2 shows time-resolved spectra for  $120 \mu\text{M}$   $\text{PtCl}_4^{2-}$  aqueous solutions. Generally, aqueous solution of  $\text{PtCl}_4^{2-}$  exhibits a strong absorption peak at 216 nm arising from ligand-to-metal charge-transfer (LMCT) transition. The spectrum reveals absorbance at 216 nm and 230 nm characteristics of  $\text{PtCl}_4^{2-}$ . The intensity of these peaks decreases gradually with time and then achieves a nearly constant value at around 25 h. The decrease in absorbance is directly attributable to the hydrolysis of  $\text{PtCl}_4^{2-}$  to yield  $[\text{PtCl}_n(\text{H}_2\text{O})_{4-n}]^{2-n}$  ( $n \leq 3$ ) [40].



**Fig. 3.** Time-resolved UV-vis spectra indicating formation of G4-OH(Pt<sup>2+</sup>) complexes in a solution containing 120 μM K<sub>2</sub>PtCl<sub>4</sub> and 3 μM G4-OH with G4-OH to Pt in 1:40 molar ratio.

Fig. 3 shows the time-resolved spectra of an aqueous solution of PtCl<sub>4</sub><sup>2-</sup> (120 μM) mixed with G4-OH dendrimers (3 μM) with a molar ratio of 40:1. The reaction between G4-OH dendrimers and Pt<sup>2+</sup> is a two-step process in which PtCl<sub>4</sub><sup>2-</sup> first undergoes hydrolysis and then the hydrolyzed product complexes with tertiary amines of G4-OH dendrimer to form a covalent bond with second step as the rate-limiting process [40]. Intensity of the peaks at 216 nm and 230 nm corresponding to PtCl<sub>4</sub><sup>2-</sup> decreases gradually with time and a new peak at 250 nm begins to develop after ~7 h. The new peak arises from the ligand-to-metal charge-transfer (LMCT) from the tertiary amines of G4-OH dendrimer to bound Pt<sup>2+</sup> and continues to grow for another 45 to 72 h. Fig. 4(a) and (b) shows the absorbance peaks at 216 nm characteristics of PtCl<sub>4</sub><sup>2-</sup>, and absorbance at 250 nm characteristics of G4-OH(Pt<sup>2+</sup>) complex respectively with reaction time. The absorbance at 250 nm stabilized after 72 h reflecting the maximum complex formation of PtCl<sub>4</sub><sup>2-</sup> possible with G4-OH dendrimer.

Pt forms a complex with the internal tertiary amine groups of G4-OH dendrimer and further reduced to Pt nanoparticles. In method I, the complex form of Pt with G4-OH dendrimer is bonded with acid functionalized Vulcan XC-72 carbon by chemical bonding and is further reduced to form Pt/G4-OH-CI. On the other hand, method II describes the bonding between Pt nanoparticle encapsulated G4-OH dendrimer with acid functionalized Vulcan XC-72 carbon. For comparison, Pt nanoparticles grown on same carbon support without dendrimers is also prepared. Pt loading as high as 15 wt% is obtained on carbon without dendrimers. By contrast, Pt

loadings of 9.7 wt% and 8.9 wt% are achieved using G4-OH assisted Pt nanoparticles deposition on carbon by method 1 (Pt/G4-OH-CI) and method 2 (Pt/G4-OH-CII), respectively. In the absence of dendrimer, higher quantity of Pt with large particle size is found to be deposited on carbon. These studies suggest that the dendrimers play an important role in controlling the Pt nanoparticle size on the carbon support.

FTIR spectra for bare G4-OH dendrimers and Pt encapsulated G4-OH dendrimers supported on carbon are shown in Fig. 5. The strong peaks at 1637 and 1556 cm<sup>-1</sup> are assigned to the characteristic amide I (C=O stretching) and amide II (C–N stretching and C–N–H bending) of the G4-OH dendrimer, respectively. Similar bands are present in Pt/G4-OH-CI, Pt/G4-OH-CII representing the successful incorporation of dendrimers in the composites. Band at 3089 cm<sup>-1</sup> is assigned to a resonance-enhanced overtone of the amide II, whereas the relatively weak band at 1245 cm<sup>-1</sup> is due to opening of the C–N–H group (amide III) [41]. The additional bands observed for dendrimers correspond to C–H deformations and C–C backbone skeletal vibrations. The asymmetric and symmetric stretching vibrations for methylene C–H bonds are observed at 2936 cm<sup>-1</sup> and 2825 cm<sup>-1</sup>, respectively. Same peaks are also observed for carbon supports. Finally, the weak doublet at 1157 cm<sup>-1</sup> and 1128 cm<sup>-1</sup> are assigned to skeletal C–C stretching in all the compounds. Peak at 1025 cm<sup>-1</sup> observed in carbon support, Pt/G4-OH-CI and Pt/G4-OH-CII are assigned to C=O stretching in carboxylate group. The presence of carboxylate group is confirmed by a peak at 1740 cm<sup>-1</sup> which shows the linkage of dendrimers with carbon. The peak has a lower intensity and is probably overlaps with the predominant amide I band in the same region. A broad band at ~3500 cm<sup>-1</sup> represents the O–H stretching of the G4-OH dendrimers and overlaps with the broad band due to the presence of water.

From the electron diffraction pattern shown in Fig. 6(d), the characteristic inter-planar spacing, *d*, between planes of Pt atoms inside dendrimers are measured. Patterns of local electron diffraction contain broadened rings due to the small size of the Pt particles and correspond to inter-planar spacing of *d*(1 1 1)=0.225, *d*(2 0 0)=0.193, *d*(2 2 0)=0.138 and *d*(3 1 1)=0.116 nm. The distances are found to be very close to inter-planar spacing observed for face centred cubic (fcc) structure showing the formation of crystalline Pt nanoparticles [42]. TEM images shown in Fig. 6(a) and (b), reveal that G4-OH encapsulated Pt nanoparticles on carbon are well-dispersed and are almost spherical in shape. Diameters of the metal particles for Pt/G4-OH-C are ≤2 nm. Fig. 6(c) represents the Pt dispersion on the surface of carbon in the absence of dendrimers. Here sizes of Pt nanoparticle varied in the range between 1 nm and 3 nm with fewer agglomerations in some region as compared to Pt/G4-OH-CI and Pt/G4-OH-CII. The corresponding histogram

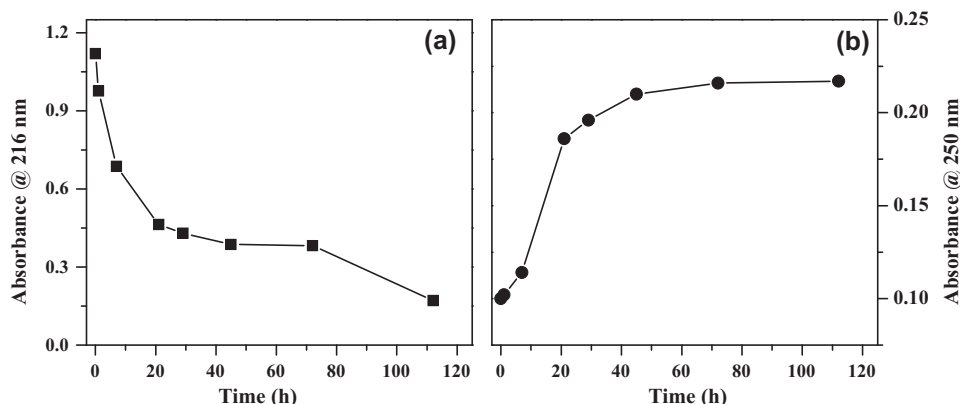


**Fig. 4.** Plots for (a) absorbance at  $\lambda = 216$  nm for PtCl<sub>4</sub><sup>2-</sup> and (b) absorbance at  $\lambda = 250$  nm for the G4-OH(Pt<sup>2+</sup>) complexes as a function of time.

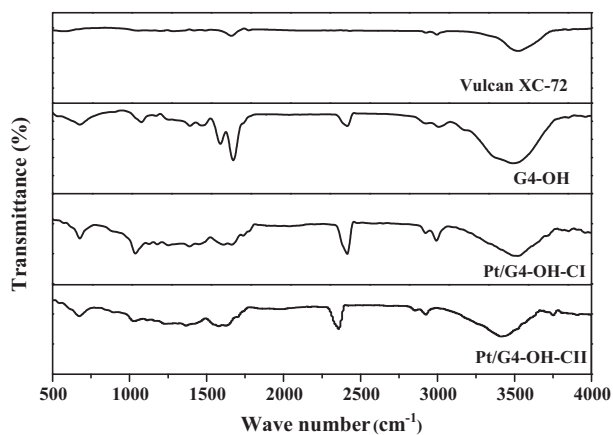


Fig. 5. FTIR spectra of Vulcan XC-72, G4-OH, Pt/G4-OH-Cl and Pt/G4-OH-CII.

active electrochemical surface area (ESA) of Pt has been evaluated from the Eq. (1).

$$ESA = \frac{Q_H}{M_{Pt} Q_{Href}} \quad (1)$$

In Eq. (1),  $Q_H$  is the amount of charge for electrochemical adsorption/desorption of hydrogen atoms on the Pt surface, and  $M_{Pt}$  is the Pt loading on electrode ( $\text{g m}^{-2}$ ).  $Q_{Href}$  is assumed to be  $0.21 \text{ mC cm}^{-2}$  corresponding to a surface density of  $1.3 \times 10^{15} \text{ atom cm}^{-2}$  of Pt [43]. ESA for Pt/G4-OH-Cl (9.7 wt%) and Pt/G4-OH-CII (8.9 wt%) are around  $76$  and  $70 \text{ m}^2 \text{ g}^{-1}$ , respectively, which is higher than the ESA value of  $63 \text{ m}^2 \text{ g}^{-1}$  for Pt/C catalyst (15 wt%). Higher ESA for Pt/G4-OH-Cl and Pt/G4-OH-CII are attributable to Pt with smaller particle size and wide-spread distribution. Furthermore, in case of Pt/C some Pt nanoparticles of  $\leq 2 \text{ nm}$  could form in the micro pores present in the carbon substrate. On the other hand, Pt particles of size  $\leq 2 \text{ nm}$  encapsulated in the dendrimer cavity exhibit better ESA values due to the larger particle size of fourth-generation G4-OH dendrimers [44] which are constrained to get into the micropores of carbon substrate. Consequently, deposition of Pt particles in the reactant non-access area of carbon could be prevented to a large extent. Therefore, the present strategy gives better Pt active area thereby improved Pt utilization albeit low deposition of Pt particles on the composite.

ORR activity for Pt/G4-OH-C composites and Pt/C are studied using RDE voltammetry conducted in a three-electrode electrochemical cell in  $0.5 \text{ M HClO}_4$ . Activity of the catalysts had been extracted from the hydrodynamic voltammogram with a scan rate

shown in Fig. 7 reveals narrow particle size distribution in the range between  $1 \text{ nm}$  and  $2.25 \text{ nm}$  for Pt/G4OH-Cl and Pt/G4OH-CII composites. However, the range lies in between  $1.5 \text{ nm}$  and  $3 \text{ nm}$  for the Pt/C without dendrimer. It is noteworthy that the presence of dendrimer helps in controlling the particle size of Pt to a narrow range and is beneficial in increasing the catalyst utilization.

Cyclic voltammograms of Pt/C, Pt/G4-OH-Cl, and Pt/G4-OH-CII in  $0.5 \text{ M HClO}_4$  at a scan rate of  $50 \text{ mV s}^{-1}$  are presented in Fig. 8. The

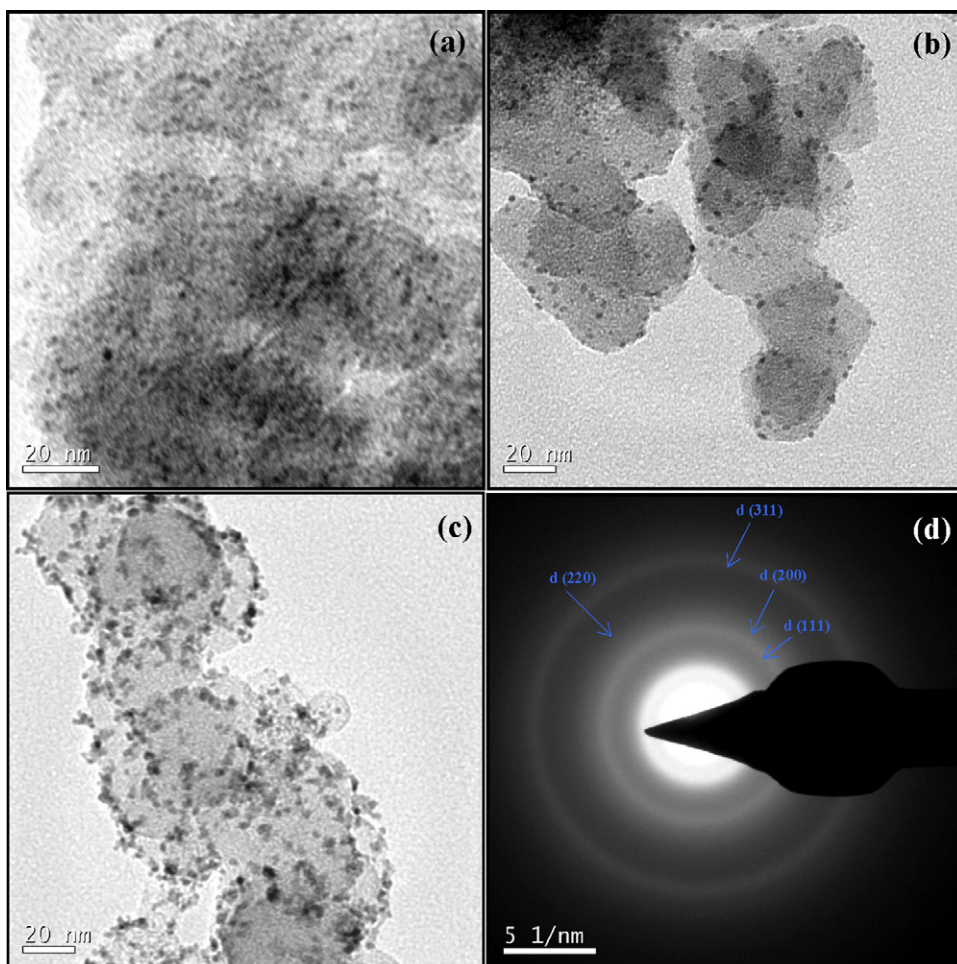


Fig. 6. TEM image of (a) Pt/G4-OH-Cl, (b) Pt/G4-OH-CII, (c) Pt/C and (d) the diffraction pattern of Pt/G4-OH-Cl.

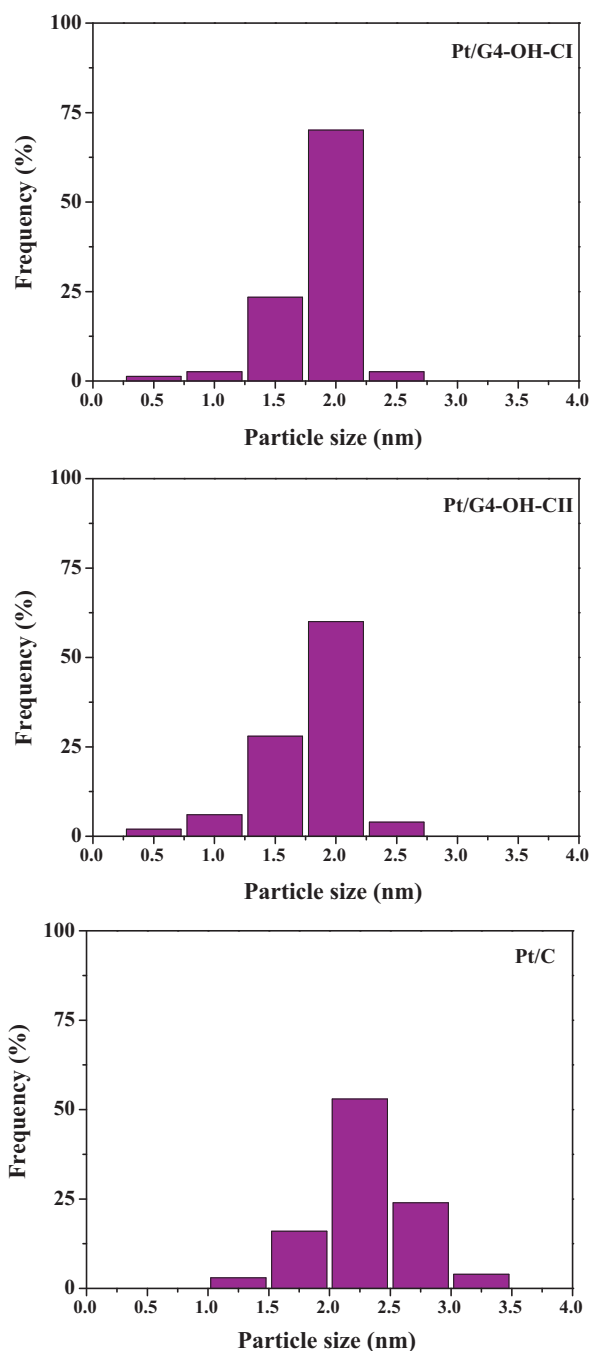


Fig. 7. Particle size distribution histogram for Pt/G4-OH-Cl, Pt/G4-OH-CII and Pt/C.

of  $2\text{ mV s}^{-1}$  at an electrode rotation of 1600rpm as shown in Fig. 9. All three samples displayed significant ORR activity along with well-defined control regions, namely kinetic, mixed, and diffusion limited, as expected with platinum-containing materials. The improved ORR kinetics for Pt/G4-OH-C is clearly visible from the respective polarization profile. Pt/G4-OH-C displayed superior ORR activity compared to Pt/C in both half-wave potential and diffusion-limited current densities. In particular, half-wave potential for Pt/G4-OH-Cl, Pt/G4-OH-CII and Pt/C are 0.89 V, 0.88 V and 0.85 V, respectively. Accordingly, the increase in ORR activity of the Pt/G4OH-C composites can be attributed to well-dispersed uniform-sized Pt nanoparticles as observed by TEM images and high ESA values for the samples mentioned. This further confirms that dendrimers are highly permeable to reactants and do not passi-

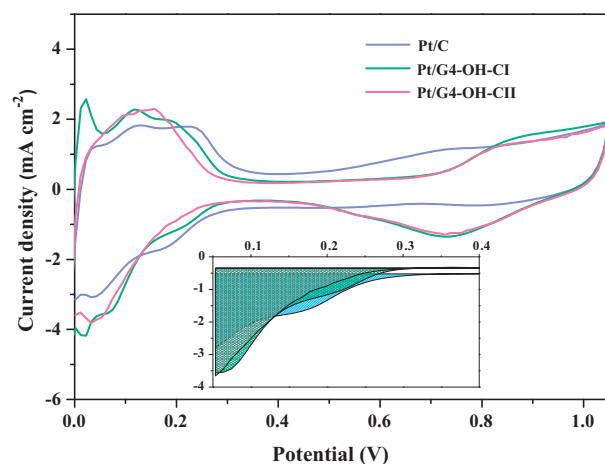


Fig. 8. CVs for Pt/G4-OH-Cl, Pt/G4-OH-CII and Pt/C recorded with 0.5 M  $\text{HClO}_4$  as the electrolyte at a scan rate of  $50\text{ mV s}^{-1}$ .

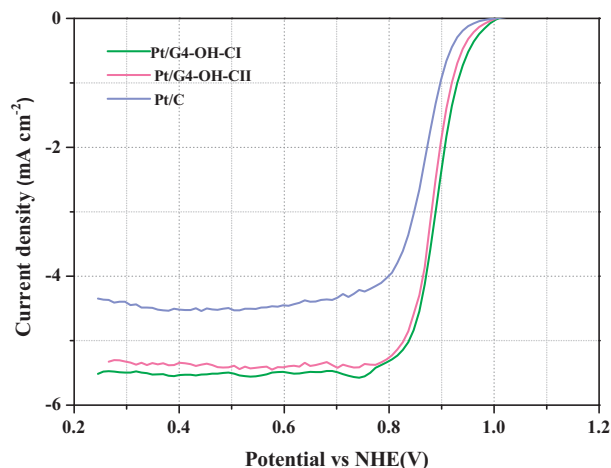


Fig. 9. Polarization data for the ORR on Pt/C, Pt/G4-OH-Cl and Pt/G4-OH-CII composites supported on a glassy carbon electrode immersed in an  $\text{O}_2$ -saturated 0.5 M  $\text{HClO}_4$  solution. The rotation rate during the experiment is 1600 rpm, and the scan rate is  $2\text{ mV s}^{-1}$ .

vate the surface of encapsulated Pt nanoparticles [18,45]. Moreover, the electrocatalytic response shows the improved electronic interactions of Pt/G4-OH-C with the carbon support.

To determine the mass activity ( $i_m$ ) of the catalysts, the polarization plot for RDE has been corrected for mass-transport [22] using the following Eq. (2).

$$i_k = \frac{i_L i}{i_L - i} \quad (2)$$

In Eq. (2),  $i_k$  is the mass-transport corrected kinetic current density,  $i_L$  is the measured diffusion limited current density, and  $i$  is the measured current density. To avoid the inaccuracy of RDE mass-transport corrections at higher current-density values, mass activity for all the catalysts are taken at 0.9 V and evaluated. The  $i_k$  values for the samples at 0.9 V are found to be  $-3.9\text{ mA cm}^{-2}$  for Pt/G4-OH-Cl,  $-2.8\text{ mA cm}^{-2}$  for Pt/G4-OH-CII, and  $-1.1\text{ mA cm}^{-2}$  for Pt/C. The  $i_k$  values normalized to mass of Pt in the electrode are plotted against the potential which is characteristic of kinetic control region as shown in Fig. 10. The extracted electrochemical parameters are presented in Table 1. Higher mass activity and specific activity ( $i_s$ ) for Pt/G4-OH-C is attributed to the higher dispersion of Pt nanoparticles and improved interaction of nanoparticle with the support. Better dispersion of uniform Pt nanoparticles is achieved by G4-OH dendrimers. In case of Pt/C, the

**Table 1**  
Kinetic current ( $i_k$ ), specific activities ( $i_s$ ) and mass activities ( $i_m$ ) for the ORR at 0.9V at ambient temperature (25 °C) determined at a rotation rate of 1600 rpm and at scan rate of 2 mV s<sup>-1</sup> from 1 to 0V (RHE).

Catalyst	ESA (m <sup>2</sup> g <sup>-1</sup> )	$E_{1/2}$ (V)	$i_k$ (mA cm <sup>-2</sup> )	$i_m$ (A mg <sub>Pt</sub> <sup>-1</sup> )	$i_s$ (μA cm <sub>Pt</sub> <sup>-2</sup> )
Pt/C	63	0.85	1.1	0.03	48
Pt/G4-OH-CI	76	0.89	3.9	0.11	140
Pt/G4-OH-CII	70	0.88	2.8	0.08	110

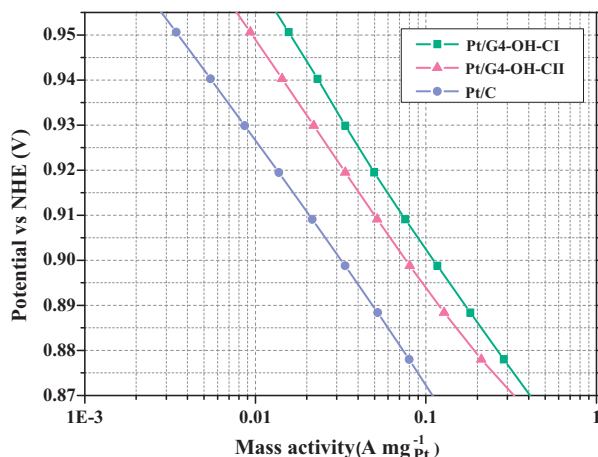


**Fig. 10.** Mass activity for Pt/C, Pt/G4OH-CI and Pt/G4OH-CII in the kinetic control region of the ORR polarization.

Pt nanoparticles are entrapped in the deep recesses of micropores of the carbon support which are hardly accessible to the reactants and restrict their participation in electrochemical reactions [46]. On the other hand, the preformed dendrimer encapsulated Pt nanoparticles could deposit on the exterior surface or in the mesopores of carbon since they are bigger in size than the micro-pore openings in the carbon. This is represented by the schematic diagram of the catalyst structures for both Pt/C and Pt/G4-OH-C (Fig. 11). Pt utilization is therefore increased in case of Pt/G4-OH-C by easy access of reactant and the electrolyte as also observed from CV and RDE studies.

In order to examine the fuel cell performance and Pt utilization, Pt/G4-OH-C composites and Pt/C were evaluated as cathode catalysts in the MEAs. Total catalyst loading for all the samples is limited to ~1.25 mg cm<sup>-2</sup>. Pt loadings in Pt/G4-OH-CI and Pt/G4-OH-CII cathodes are found to be 0.121 mg<sub>Pt</sub> cm<sup>-2</sup> and 0.111 mg<sub>Pt</sub> cm<sup>-2</sup> respectively while it is 0.188 mg<sub>Pt</sub> cm<sup>-2</sup> for Pt/C. Fig. 12 shows the

PEFC polarization and power density data recorded in H<sub>2</sub>-O<sub>2</sub> cell at 60 °C and ambient pressure. The PEFCs comprising Pt/G4-OH-CI and Pt/G4-OH-CII deliver current densities of 240 mA cm<sup>-2</sup> and 190 mA cm<sup>-2</sup>, respectively, at a cell voltage of 0.8 V. The performance is higher than that for the PEFC with Pt/C which delivers current density of only 90 mA cm<sup>-2</sup> at 0.8 V. Higher current-density observed for Pt/G4OH-C composite catalysts implies higher catalytic activity. In the catalyst layer, there are limitations to establish enough contact of catalyst and ionomer in case of Pt/C, wherein the Pt particles are buried inside the micropores of carbon, leading to the anticipated reduction in performance in relation to Pt/G4-OH-C composites. By contrast, in the case of dendrimer encapsulated Pt nanoparticles supported carbon exhibits enhanced three-phase contact with the ionomer and reactants as also observed from the ESA values discussed in earlier section. The peak power densities of 830 mW cm<sup>-2</sup> and 700 mW cm<sup>-2</sup> are found for Pt/G4-OH-CI and Pt/G4-OH-CII, respectively, while it is only 570 mW cm<sup>-2</sup> for Pt/C catalyst. Furthermore, in order to quantify the Pt utilization, the performance was re-plotted vs. unit of Pt mass as shown in Fig. 13. It can be seen that the mass activities (A mg<sub>Pt</sub><sup>-1</sup>) for Pt/G4-OH-CI and Pt/G4-OH-CII are increased by a factors of 2.2 and 2.1, respectively, at 0.4V in relation to Pt/C catalyst. Improvement in mass activity for Pt/G4-OH-C catalysts is mainly due to the contribution of ORR active sites and also due to the smaller particle size of Pt encapsulated in dendrimers. Moreover, the low pH in fuel cell environment makes all the amide groups to get protonated leading to ameliorated ionic conduction inside the dendrimer cavity which enhances Pt utilization.

It is surmised that dendrimer-encapsulated-Pt nanoparticles provide greater control of metal nanoparticles sizes, better distribution of the active phase, and ability to deposit preformed metal nanoparticles with identical size and composition on the support material. Catalytic activity of Pt/G4-OH-C synthesised by two routes are almost same and exhibits better performances in relation to Pt/C observed from ESA and ORR activity studies. It is noteworthy that reducing Pt loading without losing the PEFC performance is of utmost importance as Pt is a rare and expensive metal. Further

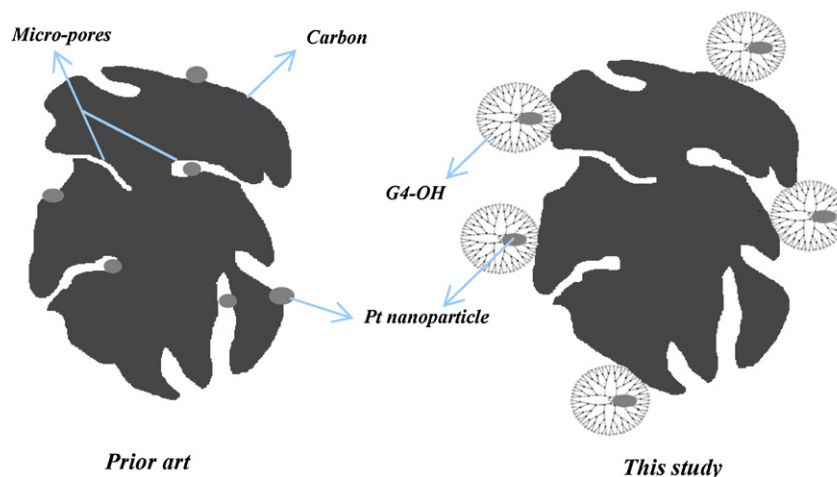


**Fig. 11.** Schematic representation of Pt loaded carbon particle in Pt/C and Pt/G4-OH-C.

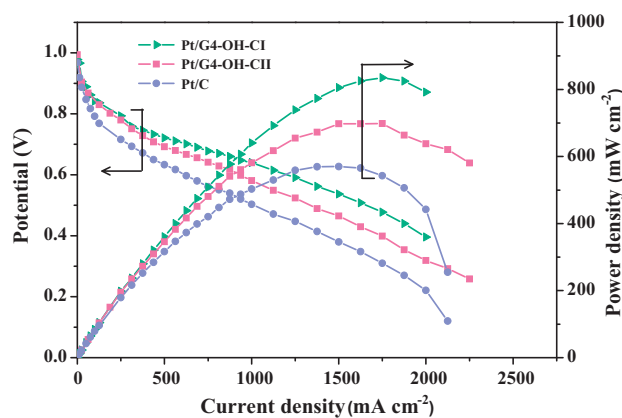


**Fig. 12.** Fuel cell polarization data for Pt/C, Pt/G4-OH-Cl and Pt/G4-OH-CII as cathode catalysts using  $\text{H}_2\text{-O}_2$  at cell temperature of  $60^\circ\text{C}$  with Nafion-212 as polymer electrolyte membrane.

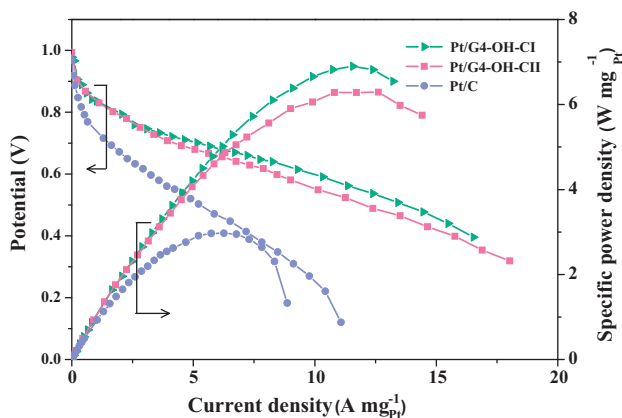


**Fig. 13.** Fuel cell polarization data for Pt/C, Pt/G4-OH-Cl and Pt/G4-OH-CII cathode catalysts represented by mass specific current and power.

improvements in PEFC performance are highly likely by increasing the Pt loading in the catalyst by immobilising more number of Pt encapsulated dendrimers on carbon support wherein the Pt particle size and agglomeration are controlled.

#### 4. Conclusions

Facile methods for preparing catalytically active carbon-supported Pt catalysts are demonstrated. The choice of PAMAM G4-OH dendrimer template provides size-controlled preparation of the Pt-based catalysts and facilitates the uniform dispersion and loading of the catalysts onto carbon supports with high activity towards ORR. Since dendrimer encapsulated Pt particles can be controlled uniformly and characterized thoroughly; studies of this nature will foster to utilize better corrosion resistant carbon supports for understanding the role of carbon on catalytic efficiency, catalyst utilization, and catalyst stability.

#### Acknowledgments

Financial support from CSIR, New Delhi, under DU-OLP-0058 (EMPOWER Scheme) and SIP-18 are gratefully acknowledged. We

thank Professor A.K. Shukla for a critical reading of the manuscript and many helpful discussions.

#### References

- [1] B.C. Steel, A. Heinzel, *Nature* 414 (2001) 345–352.
- [2] C. Ashhart, E. Uggerud, *Chem. Commun.* (2006) 2581–2582.
- [3] Y. Sun, L. Zhuang, J. Lu, X. Hong, P. Liu, *J. Am. Chem. Soc.* 129 (2007) 15465–15467.
- [4] Y. Verde, G. Alonso-Nunez, M. Miki-Yoshida, M. Jose-Yacaman, V.H. Ramos, A. Keer, *Catal. Today* 107–108 (2005) 826–830.
- [5] F. Raimondi, G.G. Scherer, R. Koz, A. Wokaun, *Angew. Chem. Int. Ed.* 44 (2005) 2190–2209.
- [6] P.J. Ferreira, G.J. la O', Y. Shao-Horn, D. Morgan, R. Makharia, S. Kocha, H.A. Gasteiger, *J. Electrochem. Soc.* 152 (2005) A2256–A2271.
- [7] S. Berchmans, P. Arunkumar, S. Lalitha, V. Yegnanarayanan, S. Bera, *Appl. Catal. B* 88 (2009) 557–563.
- [8] F. Zeng, S.C. Zimmerman, *Chem. Rev.* 97 (1997) 1681–1712.
- [9] A.W. Bosman, H.M. Janssen, E.W. Meijer, *Chem. Rev.* 99 (1999) 1665–1688.
- [10] B.J. Auten, H. Lang, B.D. Chandler, *Appl. Catal. B* 81 (2008) 225–235.
- [11] M. Fisher, F. Vogtle, *Angew. Chem. Int. Ed.* 38 (1999) 884–905.
- [12] A.I. Cooper, J.D. Londono, G. Wignall, J.B. McClain, E.T. Samulski, J.S. Lin, A. Dobrynin, M. Rubinstein, A.L.C. Burke, J.M.J. Fréchet, J.M. DeSimone, *Nature* 389 (1997) 368–371.
- [13] R.M. Crooks, M. Zhao, L. Sun, V. Chechik, L.K. Yeung, *Acc. Chem. Res.* 34 (2001) 181–190.
- [14] M.F. Ottaviani, F. Montalti, N.J. Turro, D.A. Tomalia, *J. Phys. Chem. B* 101 (1997) 158–166.
- [15] M. Zhao, L. Sun, R.M. Crooks, *J. Am. Chem. Soc.* 120 (1998) 4877–4878.
- [16] H. Ye, R.M. Crooks, *J. Am. Chem. Soc.* 127 (2005) 4930–4934.
- [17] H. Lang, R.A. May, B.L. Iversen, B.D. Chandler, *J. Am. Chem. Soc.* 125 (2003) 14832–14836.
- [18] H. Ye, R.M. Crooks, *J. Am. Chem. Soc.* 129 (2007) 3627–3633.
- [19] S. Litster, G. McLean, *J. Power Sources* 130 (2004) 61–76.
- [20] F. Barbir, S. Yazici, *Int. J. Energy Res.* 32 (2008) 369–378.
- [21] D. Wang, S. Lu, Y. Xiang, S.P. Jiang, *Appl. Catal. B* 103 (2011) 311–317.
- [22] H.A. Gasteiger, S.S. Kocha, B. Sompalli, F.T. Wagner, *Appl. Catal. B* 56 (2005) 9–35.
- [23] E. Antolini, *Appl. Catal. B* 100 (2010) 413–426.
- [24] S.Y. Huang, P. Ganesan, B.N. Popov, *Appl. Catal. B* 93 (2009) 75–81.
- [25] G.G. Wildgoose, C.E. Banks, R.G. Compton, *Small* 2 (2006) 182–193.
- [26] M. Schulz-Dobrick, K.V. Sarathy, M. Jansen, *J. Am. Chem. Soc.* 127 (2005) 12816–12817.
- [27] I. Hussain, S. Graham, Z. Wang, B. Tan, D.C. Sherrington, S.P. Rannard, A.I. Cooper, M. Brust, *J. Am. Chem. Soc.* 127 (2005) 16398–16399.
- [28] K.K. Tintula, A.K. Sahu, A. Shahid, S. Pitchumani, P. Sridhar, A.K. Shukla, *J. Electrochem. Soc.* 157 (2010) B1679–B1685.
- [29] K.K. Tintula, A.K. Sahu, A. Shahid, S. Pitchumani, P. Sridhar, A.K. Shukla, *J. Electrochem. Soc.* 158 (2011) B622–B631.
- [30] J.F.G.A. Jansen, E.M.M. de Brabander-van den Berg, E.W. Meijer, *Science* 266 (1994) 1226–1229.
- [31] L. Balogh, D.A. Tomalia, *J. Am. Chem. Soc.* 120 (1998) 7355–7356.
- [32] K. Esumi, R. Nakamura, A. Sujuki, K. Torigoe, *Langmuir* 16 (2000) 7842–7846.
- [33] M. Zhao, R.M. Crooks, *Angew. Chem. Int. Ed.* 38 (1999) 364–366.
- [34] M. Zhao, R.M. Crooks, *Adv. Mater.* 11 (1999) 217–220.
- [35] V. Chechik, M. Zhao, R.M. Crooks, *J. Am. Chem. Soc.* 122 (2000) 1243–1244.
- [36] T. Maiyalagan, *J. Solid State Electrochem.* 13 (2009) 1561–1566.
- [37] R.W.J. Scott, H. Ye, R.R. Henriquez, R.M. Crooks, *Chem. Mater.* 15 (2003) 3873–3878.
- [38] O.S. Alexeev, A. Siani, G. Lafaye, C.T. Williams, H.J. Ploehn, M.D. Amiridis, *J. Phys. Chem. B* 110 (2006) 24903–24914.
- [39] L.F. Grantham, T.S. Elleman, D.S. Martin Jr., *J. Am. Chem. Soc.* 77 (1955) 2965–2971.
- [40] M.R. Knecht, M.G. Weir, V.S. Myers, W.D. Pysz, H. Ye, V. Petkov, D.J. Buttrey, A.I. Frenkel, R.M. Crooks, *Chem. Mater.* 20 (2008) 5218–5228.
- [41] D.S. Deutsch, A. Siani, P.T. Fanson, H. Hirata, S. Matsumoto, C.T. Williams, M.D. Amiridis, *J. Phys. Chem. C* 111 (2007) 4246–4255.
- [42] T.K. Zvonareva, A.A. Sitnikova, G.S. Frolova, V.I. Ivanov-Omskioe, *Semiconductors* 42 (2008) 325–328.
- [43] G. Faubert, D. Guay, J.P. Dodelet, *J. Electrochem. Soc.* 145 (1998) 2985–2992.
- [44] R.W.J. Scott, O.M. Wilson, R.M. Crooks, *J. Phys. Chem. B* 109 (2005) 692–704.
- [45] J.C. Garcia-Martinez, R. Lezutekong, R.M. Crooks, *J. Am. Chem. Soc.* 127 (2005) 5097–5103.
- [46] D. Zhao, B. Xu, *Angew. Chem. Int. Ed.* 118 (2006) 5077–5081.